

# Goodness of Fit in Nonlinear Dynamics: Mis-specified Rates or Mis-specified States?

Giles Hooker and Stephen P. Ellner

June 24, 2022

## Abstract

This paper introduces tests to uncover the nature of lack of fit in ordinary differential equation models (ODEs) proposed for data. We present a hierarchy of three possible sources of lack of fit: unaccounted-for stochastic variation, mis-specification of functional forms in the rate equations, and missing dynamical variables in the description of the system. We represent lack of fit by allowing some parameters to vary over time, and propose generic testing procedures that do not rely on specific alternative models. Our hypotheses are expressed in terms of nonparametric relationships among latent variables, and the tests are carried out through a combined residual bootstrap and permutation methods. We demonstrate the effectiveness of these tests on simulated data, and on real data from laboratory ecological experiments and electro-cardiogram data.

## 1 Introduction

Recent statistical literature has seen substantial interest in the problem of fitting nonlinear continuous-time dynamical systems to data. Statistical problems include estimating parameters, determining parameter identifiability, experimental design and testing goodness of fit. These topics have been approached from numerous perspectives and using various models, from deterministic models in the form of ordinary differential equations (ODEs) through stochastic models based on Wiener processes or finite population models. Techniques for fitting models include nonlinear least squares (Bock, 1983; Bates and Watts, 1988; Arora and Biegler, 2004; Girolami et al., 2011), maximizing likelihoods for stochastic systems through particle filters (Ionides et al., 2006) or via equivalent Bayesian methods (e.g. Golightly and Wilkinson, 2011), methods based on pre-smoothing (Bellman and Roth, 1971; Varah, 1982; Ellner et al., 2002; Wu et al., 2012), mimicking forecast models (Pascual and Ellner, 2000) or indirect inference (Gouriéroux and Monfort, 1997), and fitting summary statistics (Tien and Guckenheimer, 2008; Ratmann et al., 2009; Reuman et al., 2006; Wood, 2010). Ramsay et al. (2007) combines the criteria from least squares and from pre-smoothing methods to achieve the advantages of each.

This paper presents an approach to model diagnostics for improving the fit of a dynamical systems model. Hooker (2009) proposed a goodness of fit test for ODE models using a likelihood ratio test. Here we assume that a proposed ODE model has been found to fit poorly, and attempt to distinguish among different potential sources of model mis-specification. In particular, we suppose that an ordinary differential equation model:

$$\frac{d}{dt}\mathbf{x} = \mathbf{f}(\mathbf{x}; t, \boldsymbol{\theta}) \quad (1)$$

has been posited in which  $\mathbf{x} \in \mathbb{R}^d$  describes the state of the system and  $\mathbf{f}(\mathbf{x}; t, \boldsymbol{\theta})$  describes how quickly the system changes at location  $\mathbf{x}$  in state-space. We assume that we have vector-valued data  $\mathbf{y}_1, \dots, \mathbf{y}_n$  from this system observed at times  $t_1, \dots, t_n$  where  $\mathbf{y}_i$  is related to  $\mathbf{x}(t_i)$  by a known, possibly indirect, measurement process. If we find the model cannot fit the data well, we then wish to improve the fit

somehow. Here, we develop testing methods to distinguish between three likely reasons for lack of fit, which would imply three different directions for improving the model:

1. Un-modeled disturbances unrelated to system dynamics, which if modelled as random suggests a probabilistic description of system dynamics;
2. Mis-specification of the parametric form of  $\mathbf{f}$ ;
3. Mis-specification of the state vector  $\mathbf{x}$ , in particular that the state vector  $\mathbf{x}$  omits some variables that are needed to provide a full description of the system state.

The methods we propose are broadly applicable to model improvement in systems which are explicitly stochastic in proposing a probabilistic model for the evolution of  $\mathbf{x}$ . However, tests involving such systems will require modifications to some of the details below and we will not examine these further.

Hooker (2009) notes that residuals from solutions to ordinary differential equations give poor graphical indications of how lack of fit may be addressed. This is because differential equation models describe the derivatives  $d\mathbf{x}/dt$  rather than the (observed) state variables themselves. Instead, Hooker (2009) proposed estimating lack of fit as *empirical forcing functions*. These are non-parametric functions  $\mathbf{g}(t)$  modifying (1) to

$$\frac{d}{dt}\mathbf{x}(t) = \mathbf{f}(\mathbf{x}(t); t, \theta) + \mathbf{g}(t) \quad (2)$$

so that a good fit to the data is achieved.  $\mathbf{g}(t)$  will thus represent both random disturbances to the system and deterministic lack of fit. The advantage of this representation is that a graphical exploration of  $\mathbf{g}(t)$  provides a visual indication of how  $\mathbf{f}$  may be modified to improve fit. Hooker (2009) provides approximate goodness-of-fit tests for the null hypothesis  $\mathbf{g} \equiv 0$  based on a basis-expansion:  $\mathbf{g} = \Psi(t)D$  for a vector of basis functions  $\Psi(t)$  and a coefficient matrix  $D$ .

In this paper, we take the same approach but expand the ways in which we may model lack of fit to include allowing some parameter to change over time, producing the system

$$\frac{d}{dt}\mathbf{x}(t) = \mathbf{f}(\mathbf{x}(t); \theta, \mathbf{g}(t)) \quad (3)$$

in which  $\mathbf{g}(t)$  can modify  $\mathbf{f}$  more generally than by additive forcing. In particular, we will examine allowing a parameter of interest to vary over time when doing so has a relevant, mechanistic interpretation. The calculations in Hooker (2009) – based on first-order Taylor expansions – can be readily extended to test  $\mathbf{g}(t) \equiv 0$  in this case. This approach can be seen as encompassing the model (2) and we will use it throughout the paper.

Our new diagnostic tests provide more information about that nature of the lack of fit when  $\mathbf{g}(t)$  is found to be significant. In particular, three nested possibilities for the properties of  $\mathbf{g}(t)$  correspond to the alternatives listed above for how model (1) should be reformulated:

1. Exogenous stochastic perturbations: if  $\mathbf{g}(t)$  is independent of  $\mathbf{x}(t)$ , this suggests that  $\mathbf{g}(t)$  be modeled as a stochastic process, but that the functional form of (1) is otherwise reasonable.
2. Mis-specification of  $\mathbf{f}$ : this is indicated by  $\mathbf{g}(t)$  being at least partly determined by  $\mathbf{x}(t)$ . This would require  $\mathbf{f}$  to be revised, as already discussed in Hooker (2009).
3. Missing state variables: if  $\mathbf{g}(t)$  depends not only on  $\mathbf{x}(t)$  but also on past values  $\mathbf{g}(t - \delta)$ . These lags serve as surrogates for missing state variables such as additional species in an ecological model, additional chemical products in a reaction or additional ion channels in a neuron.

In this paper, we develop tests to distinguish between each successive pair of possibilities. These tests need to account for sources of variation that include resampling methods for the  $\mathbf{y}_t$  as well as examining the significance of an appropriate non-parametric regression.

To provide a concrete example, we consider a model and data from experimental population ecology. In the actual experiments (Becks et al., 2010) algae of the species *Chlamydomonas reinhardtii*,

( $C$ ) are grown in a chemostat microcosm which is continuously supplied with nitrogen-limited medium. These algae are preyed upon by rotifers of the species *Brachionus calyciflorus* ( $B$ ), near-microscopic animals that feed on algae and reproduce asexually unless at high population density. As a candidate model for this system, we use a standard predator-prey model from the ecological literature, the Rosenzweig-MacArthur model:

$$\begin{aligned}\frac{dC}{dt} &= rC \left(1 - \frac{C}{K_C}\right) - \frac{pGCB}{K_B + pC} \\ \frac{dB}{dt} &= \frac{\chi_B p G C B}{K_B + pC} - \delta B.\end{aligned}\tag{4}$$

Here  $dC/dt$  is the rate of change of the algal population. The first equation describes this change in terms of logistic growth (because algae are limited by resource constraints) with maximal growth rate  $r$  and carrying capacity  $K_C$ . This term represents algal birth rate minus deaths for causes unrelated to predation (in the actual experiments, washout from the chemostat is the main cause of algal mortality). The second term represents predation by rotifers. Predation occurs at maximum rate  $G$  but is reduced when algae are scarce, with  $K_B$  representing the algal density  $pC$  at which the predation rate is half of its maximum. The parameter  $p$  represents the fraction of algae available for predation, and is held at 1 for the moment. Later we will allow  $p$  to vary with time, in providing goodness of fit diagnostics. The equation for the rotifer growth rate  $dB/dt$  represents the conversion of consumed algae into rotifers with conversion rate  $\chi_B$ , and rotifer mortality  $\delta B$  in proportion to their numbers. Numerically, it is advantageous to re-express this system in terms of log variables  $\tilde{\mathbf{x}} = (\log C, \log B)$  with differential equation  $d\tilde{\mathbf{x}}/dt = \mathbf{f}(\exp(\tilde{\mathbf{x}}); t, \boldsymbol{\theta}) / \exp(\tilde{\mathbf{x}})$  and we have employed this below.

The experimental system was sampled once each day, and rotifers and algae in the sample were counted. Two samples were taken each day, from the top and bottom of the chemostat, to verify that the system was well-mixed so that spatial variation in population densities does not need to be considered. The data we analyze are the average of the two daily samples. Plots of the time series and a fit to these data are given in the first panel of Figure 1; these data come from Becks et al. (2010), where the experimental methods are presented in detail.

A number of features are evident from these plots. Most evidently, solutions to the ODE have much more regular cycles than the observed time series. There is also a difference in phase relationships between the rotifers and algae. In the ODE solutions the rotifer peak is about 1/4 cycle period delayed from the algal peak (because rotifer *population growth rate* peaks when algal density is at a maximum), but in the observed time series the delay is about 1/2 the cycle period. A proposed explanation for this discrepancy (Yoshida et al., 2003) is that the algae consist of two populations: one of which does not get predated but pays a cost in reproducing less efficiently, so that the relative advantage of each subpopulation is determined by the rate of rotifer predation. Models incorporating subpopulation structure – hence expanding the state-vector to  $(C_1, C_2, B)$  for two algal populations – reproduce this out-of-phase dynamics (Yoshida et al., 2003). However, this does not rule out the possibility that the lack of fit is actually due to mis-specifying the functional forms for the dynamics of the two-dimensional state vector  $(C, B)$ . In our examination below, we will allow  $p$  – the proportion of  $C$  that is edible – to vary over time and examine whether this variation can be considered random (Case 1), is partly determined by  $C$  and  $B$  (Case 2), or also depends on its past history, indicating a Case 3 mis-specification. Experimental evidence tells us that the right answer is Case 3 (Yoshida et al., 2003): when the algal population is homogenous (all individuals descended from a single cell), the dynamics are much more like the predictions of classical predator-prey models such as (4).

In order to conduct goodness of fit tests for these data, we must first estimate parameters. In a mis-specified system, parameter estimates, even for correctly-specified terms, can be biased in ways that distort visual diagnostics. In this paper, we therefore estimate parameters through the profiling methodology of Ramsay et al. (2007). This method allows the trajectory to deviate from an ordinary differential equation, and therefore provides parameter estimates with some robustness to lack of fit.

To represent time-varying quantities  $\mathbf{g}(t)$ , we employ a basis expansion,  $\mathbf{g}(t) = \Psi(t)D$  in which the coefficients  $D$  of the basis function  $\Psi(t) = \psi_1(t), \dots, \psi_K(t)$  are treated as additional parameters to be estimated. Because the addition  $D$  can make the system unidentifiable (eg Hooker, 2009), we employ a two-stage estimation procedure, first estimating fixed parameters  $\theta$  and then obtaining an estimate for  $D$ .

While the ecological experiment described above provides a useful motivation, our diagnostics can be employed on variety of systems. We explore by simulation the effectiveness of our methods in models for cardiac rhythms and chaotic dynamics as well as the Rosenzweig-MacArthur model above. These are investigated both in cases in which simulated data are generated from an ODE and also when a stochastic differential equation is used to generate noisy trajectories which are then observed with noise.

The rest of the paper is structured as follows. Section 2 details parameter estimation methods and visual diagnostics for lack of fit and Sections 3 and 4 provide testing procedures for mis-specification of  $\mathbf{f}$  and  $\mathbf{x}$  respectively. Section 5 evaluates these procedures in distinguishing van der Pol and Rössler systems from linear ODEs while Sections 6 and 7 investigate these procedures with the non-linear Rosenzweig-MacArthur and van der Pol systems respectively along with applying them to real-world data. We conclude with some speculation about the power of these tests and further directions to be investigated.

## 2 Parameter Estimation and Visual Diagnostics

Throughout this paper we assume that an ordinary differential equation of the form (1) has been proposed for a system under study in which  $\mathbf{x}(t)$  is a  $d$ -dimensional vector and  $\mathbf{f}(t, \mathbf{x}, \theta)$  takes values in  $\mathbb{R}^d$ . We further assume that we have observations  $\mathbf{y}_i = \mathbf{x}(t_i) + \boldsymbol{\epsilon}_i$  taken at times  $t_i$ . The  $\mathbf{y}_i$  need not include measurements of all state variables and we will understand any comparisons with data to ignore unmeasured components. In many real-world cases, the  $\mathbf{y}_i$  measure a transformation of  $\mathbf{x}(t_i)$  rather than  $\mathbf{x}(t_i)$  directly. While the methods described below can be readily extended to this case, this does not occur in our examples and we will only present the directly observed case for the sake of clarity.

In order to estimate parameters in ordinary differential equations we employ the methods of Ramsay et al. (2007). These methods represent the trajectory of the system via a basis expansion:  $\mathbf{x}(t) = \Phi(t)C$  where  $\Phi(t) = (\phi_1(t), \dots, \phi_L(t))$  is a vector of basis functions and  $C$  is a  $L \times d$  matrix of coefficients. Rather than solving the ODE (1) explicitly, for each value of  $\theta$ , coefficients  $C_\lambda(\theta)$  are chosen to minimize a trade-off criterion

$$J(C, \theta) = \sum_{i=1}^n \|\mathbf{y}_i - \Phi(t_i)C\|_2^2 + \lambda \int \left\| \frac{d\Phi(t)}{dt}C - \mathbf{f}(\Phi(t)C; t, \theta) \right\|_2^2 dt.$$

Here, the norms in the above equation are understood to be possibly weighted between different variables. The first norm is also understood to ignore components of  $\mathbf{x}(t_i)$  that are not measured.

As opposed to non-parametric smoothing, we think of  $\lambda$  as being large and this choice of  $C_\lambda(\theta)$  allows the differential equation to be approximately solved with some deviation in the direction of the data. This approximate solution is then used to selected  $\theta$  as though it was a deterministic function in nonlinear least squares. That is  $\theta$  is chosen by minimizing

$$H(\theta) = \sum_{i=1}^n \|\mathbf{y}_i - \Phi(t_i)C_\lambda(\theta)\|_2^2.$$

These can be efficiently carried out using software in Hooker et al. (2010); see Ramsay et al. (2007) for implementation details.

In our methods we first estimate  $\hat{\theta}$  in the manner above with  $\mathbf{g}(t) \equiv 1$ . We then parameterize  $\mathbf{g}(t) = \Psi(t)D$  by another basis expansion and estimate  $D$  as further parameters with  $\hat{\theta}$  held fixed.

This two-stage estimation procedure is carried out to ensure the identifiability of parameters. Note that even when estimating  $D$ , we employ the profiling methodology so that the estimate  $\mathbf{x}(t)$  will not correspond to an exact ODE solution; this will also provide a visual diagnostic for the adequacy of time-varying parameters to account for lack of fit.

We can now employ the estimate  $\hat{\mathbf{g}}(t) = \Psi(t)\hat{D}$ , to visually examine lack of fit. Hooker (2009) produced an approximate test of whether  $\hat{\mathbf{g}}(t)$  differs from being constant. If it does, we can plot  $\hat{\mathbf{g}}(t)$  versus  $\hat{\mathbf{x}}(t)$  to look for consistent relationships that may indicate mis-specification of the form of  $\mathbf{f}$ . This approach is taken rather than examining the residuals  $\hat{\epsilon}_i = \mathbf{y}_i - \Phi(t_i)\hat{C}_\lambda(\hat{\theta})$  because consistent patterns in these will not necessarily indicate ways in which  $\mathbf{f}$  should be modified to account for these.

These visual diagnostics are demonstrated in Figure 1 in which the estimated  $p(t)$  appears to bear some relationship to both  $B(t)$  and  $C(t)$ , and where we can observe that even with  $p(t)$  included in the estimation, there remains some additional departure between  $d\mathbf{x}/dt$  and  $\mathbf{f}(\mathbf{x}; \theta, \mathbf{g})$ .

Our approach does not require us to employ the profiling method, however. In Section 7 we resort to gradient matching (Ellner et al., 2002) for the sake of computational efficiency when working with a frequently-sampled system. This relies on smoothing the data to obtain a nonparametric estimate  $\hat{\mathbf{x}}$  of the unobserved smooth trajectory, and then matching  $d\hat{\mathbf{x}}/dt$  to  $\mathbf{f}(\hat{\mathbf{x}}; t, \theta)$ . In the model in Section 7 our ODE is given in terms of second derivatives for a one-dimensional system. This approach can be carried out much more quickly than the profiling method – we used it in other systems to obtain initial parameter estimates – and the same calculations we develop below can be employed here as well.

### 3 Tests for Dependence Between $\mathbf{g}(t)$ and $\mathbf{x}(t)$

Assume now that  $\mathbf{g}(t)$  has been shown to differ from zero, and hence that the ODE model (1) is mis-specified. We next want to distinguish between the three alternative forms of mis-specification listed in the Introduction. The first step, to distinguish between alternatives 1. and 2., is to ask whether  $\mathbf{g}(t)$  has a consistent relationship with  $\mathbf{x}(t)$ . If so, this will indicate that the functional form of  $\mathbf{f}$  has been mis-specified, and the visual diagnostics above can help to determine how it should be amended. To determine this, we assume a null hypothesis in which  $\mathbf{g}(t)$  follows a smooth, stationary stochastic process with zero mean, and attempt to distinguish this hypothesis from non-parametric dependence of  $\mathbf{g}(t)$  on  $\mathbf{x}(t)$ . The alternative still allows for error due to genuine random disturbances, estimation errors and other forms of mis-specification. We conduct this test via a block-permutation test, using nonparametric estimates for the relationship between  $\mathbf{g}(t)$  and  $\mathbf{x}(t)$ . We also account for the estimation of  $\mathbf{g}(t)$  through a residual bootstrap.

Formally, our test can be stated as:

$$H_0 : E(\mathbf{g}(t)|\mathbf{x}(t)) \equiv 0, \forall t \text{ versus } H_A : E(\mathbf{g}(t)|\mathbf{x}(t)) \equiv \mathbf{h}(\mathbf{x}(t)) \forall t$$

This could be conducted via a generalized likelihood ratio test (Fan and Yao, 2008), but we must account for the functional nature of  $\mathbf{g}(t)$  and  $\mathbf{x}(t)$  and their estimation. An obvious alternative is to conduct a block-permutation test: permuting  $\mathbf{g}(t)$  on intervals  $[t_i, t_{i+1}]$ , solving a differential equation model with the permuted  $\mathbf{g}^b(t)$  appearing as a time-varying term, and re-estimating  $\mathbf{g}(t)$ . For large systems, this may be computationally prohibitive. By destroying the continuity of the estimated  $\mathbf{g}(t)$ , it can also induce instability in numerical ODE solvers.

Instead, we propose a two-stage procedure: 1. A block-permutation test for the a relationship between  $\mathbf{g}(t)$  and  $\mathbf{x}(t)$  will be conducted as though  $\mathbf{g}(t)$  and  $\mathbf{x}(t)$  are both fixed. 2. We will then re-sample both  $\mathbf{g}(t)$  and  $\mathbf{x}(t)$  via a residual bootstrap and repeat the permutation test. The residual bootstrap, by itself, does not reduce the computational workload. However, we propose a Taylor-series approximation to it. Let  $\hat{\mathbf{y}}$  be the expected value of the observations given  $\hat{\mathbf{x}}$  and  $\theta$ . We calculate the Taylor series expansion of  $\hat{\mathbf{y}}$  about the the coefficients  $\mathbf{d} = \text{vec}(D)$  defining the empirical forcing function  $\mathbf{g}(t)$ . We also take a first-order expansion of  $\hat{\mathbf{y}}$  about the estimated parameters  $\theta$ . This then

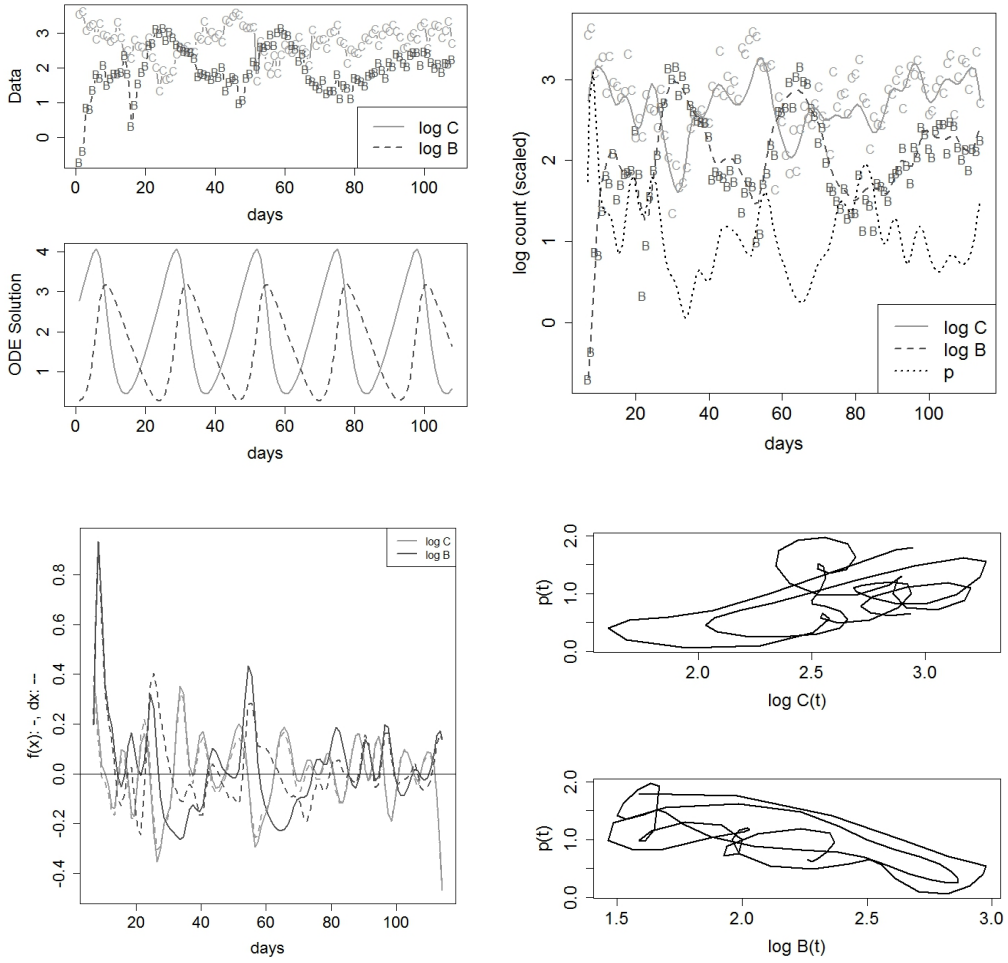


Figure 1: Diagnostics for the Chemostat Data. Top Left: log data (top) and solution to Rosenzweig-MacArthur ODE on log scale with constant  $p(t)$  (bottom). Top right: profiled trajectory including time-varying  $p(t)$ . Bottom left, comparison of  $dx/dt$  (dashed lines) and  $f(\mathbf{x}; \theta, p(t))$  (solid lines). Bottom right:  $p(t)$  plotted against  $C(t)$  and  $B(t)$ .

produces the following approximate model

$$\mathbf{y} - \hat{\mathbf{y}} = \delta_\theta \frac{d\hat{\mathbf{y}}}{d\theta} + \delta_{\mathbf{d}} \frac{d\hat{\mathbf{y}}}{d\mathbf{d}} + \epsilon. \quad (5)$$

Using this linear model, we bootstrap the residuals  $\mathbf{y} - \hat{\mathbf{y}}$  and can then cheaply obtain bootstrap estimates  $\delta_\theta^b$  and  $\delta_{\mathbf{d}}^b$  by least squares. We then update the coefficients for  $\mathbf{g}(t)$  by  $\mathbf{d}^b = \hat{\mathbf{d}} + \delta_{\mathbf{d}}^b$ , we also update the coefficients for  $\mathbf{x}$  as

$$\hat{C}^b = \hat{C}_\lambda(\theta, \mathbf{d}) + \frac{d\hat{C}_\lambda(\hat{\theta}, \hat{\mathbf{d}})}{d\theta} \delta_\theta^b + \frac{d\hat{C}_\lambda(\theta, \mathbf{d})}{d\mathbf{d}} \delta_{\mathbf{d}}^b \quad (6)$$

and use these to form  $\mathbf{g}^b(t)$  and  $\mathbf{x}^b(t)$  on which we can conduct a block permutation test.

The method above results in the following proposed algorithm:

1. Estimate  $\hat{\theta}$  by the profiling methods in Ramsay et al. (2007).
2. Estimate  $\mathbf{g}(t) = \Psi(t)\hat{D}$  with  $\hat{\theta}$  kept fixed. This may be done by treating  $\mathbf{d} = \text{vec}(D)$  as parameters in the same scheme as used to estimate  $\hat{\theta}$ .
3. Estimate  $\hat{\mathbf{y}}$  by solving (2). Let  $d\hat{\mathbf{y}}/d\theta$  and  $d\hat{\mathbf{y}}/d\mathbf{d}$  be the derivatives of  $\hat{\mathbf{y}}$  with respect to  $\theta$  and  $\mathbf{d}$  respectively; these are bi-products of the previous two steps. Let  $\hat{\epsilon}$  be the residuals of  $\mathbf{y}$  from  $\hat{\mathbf{y}}$ .
4. (Residual Bootstrap) Loop over  $b = 1, \dots, B_1$ :

- (a) Create a bootstrap response  $\mathbf{y}^b$  by resampling  $\hat{\epsilon}$ .
- (b) Obtain estimates  $\delta_{\mathbf{d}}^b$  from the model (5) and create  $\mathbf{g}^b(t)$  using  $\mathbf{d}^b = \hat{\mathbf{d}} + \delta_{\mathbf{d}}^b$  as coefficients and  $\mathbf{x}^b(t)$  by using the coefficients  $\hat{C}^b$  in (6).
- (c) Using time points  $t_1, \dots, t_K$ , let  $\tilde{\mathbf{g}}_i^b = \mathbf{g}^b(t_i)$  and  $\tilde{\mathbf{x}}_i^b = \mathbf{x}^b(t_i)$ . Estimate a model  $\mathbf{h}_1^b(\tilde{\mathbf{x}}^b)$  to predict  $\tilde{\mathbf{g}}^b$  from  $\tilde{\mathbf{x}}^b$  via nonparametric regression and let  $F_{0b}$  be the usual  $F$ -statistic for this model:

$$F_{0b} = \frac{\frac{1}{K} \sum_{i=1}^K \left\| \mathbf{h}_1^b(\tilde{\mathbf{x}}_i^b) - \frac{1}{K} \sum_{j=1}^K \mathbf{h}_1^b(\tilde{\mathbf{x}}_j^b) \right\|^2}{\frac{1}{K} \sum_{i=1}^k \left\| \tilde{\mathbf{g}}_i^b - \mathbf{h}_1^b(\tilde{\mathbf{x}}_i^b) \right\|^2}.$$

- (d) (Permutation Test) Loop over  $k = 1, \dots, B_2$ : let  $\tilde{\mathbf{g}}^{bk}$  be a block-permutation of  $\tilde{\mathbf{g}}^b$  and calculate  $F_{kb}$  to be the corresponding  $F$ -statistic for a nonparametric regression to predict  $\tilde{\mathbf{g}}^{bk}$  from  $\tilde{\mathbf{x}}_i^b$ .
- (e) Measure  $p_b = \frac{1}{B_2} \sum_{k=1}^{B_2} I(F_{0b} > F_{kb})$ .

5. Reject  $H_0$  if  $\sum_b p_b / B_1 < \alpha$ .

In Step 4d, we employ blocks that larger than the support of a the bases  $\Psi(t)$  in order to maintain the natural dependence among the  $\tilde{\mathbf{g}}^b$ . We also remove one half block at the beginning and end of time points to avoid edge effects in estimating  $\mathbf{g}$ . Nonparametric regression is obtained using smoothing splines throughout, employing 40 basis functions and the default settings in the package `mgcv` (Wood, 2013).

Note that while this scheme assumes an ODE model and uses the profiling approaches in Ramsay et al. (2007) for parameter estimation, the idea can be generalized to both explicitly stochastic systems and to alternative parameter estimation methods. However, an important practical advantage of the methods we employ is the availability the Taylor approximations used above that allow us to avoid both solving ordinary differential equations and repeatedly re-estimating parameters.

## 4 Tests for Missing Dynamical Variables

In addition to mis-specifying the parametric form of  $\mathbf{f}$ , in dynamical systems it is also possible to mis-specify  $\mathbf{x}$ . In particular, the proposed differential equation may ignore important components of a system. One example of this is presence of two visually indistinguishable sub-populations of algae in the chemostat system described in the Introduction. Another occurs in neural dynamics in which the voltage across the neuron cell membrane is governed by multiple ion channels (e.g. Tien and Guckenheimer (2008), and see Wilson (1999) for an overview). Not all of the known channels are always necessary to describe the dynamics of a single neuron, so models often focus on a subset of channels, and lack of fit may result if too few channels have been included in a model. Similar situations can arise in modeling chemical reactions or pharmacokinetics, if a model fails to include all reactions or reaction products.

In this section, we assume that we have specified a model for observed data (1) while the data, in fact, corresponds to a model of the form

$$\begin{aligned}\frac{d\mathbf{x}}{dt} &= \tilde{\mathbf{f}}(\mathbf{x}, y, \theta) \\ \frac{dy}{dt} &= k(\mathbf{x}, y)\end{aligned}$$

and we seek to determine that mis-specification of the system has this form. To carry this out, we seek to evidence that  $\mathbf{g}(t)$  has additional internal dynamics that are not accounted for by its dependence on  $\mathbf{x}(t)$ . To provide heuristic motivation for our approach, consider the additive form of lack of fit (2) with a univariate forcing term  $g(t)$  added to the equation associated with one of the state variables  $x_i$ . Then we can write

$$g(t) = \tilde{f}_i(\mathbf{x}(t), y(t), \theta) - f_i(\mathbf{x}(t), \theta)$$

Under this framework, if we examine the time derivative of  $g$ :

$$\begin{aligned}\frac{dg(t)}{dt} &= \frac{d\mathbf{x}(t)}{dt} \left[ \frac{d\tilde{f}_i(\mathbf{x}(t), y(t), \theta)}{d\mathbf{x}} - \frac{df_i(\mathbf{x}(t), y(t), \theta)}{d\mathbf{x}} \right] + \frac{dy(t)}{dt} \frac{d\tilde{f}_i(\mathbf{x}(t), y(t), \theta)}{dy} \\ &= \tilde{\mathbf{f}}(\mathbf{x}(t), y(t), \theta) \left[ \frac{d\tilde{f}_i(\mathbf{x}(t), y(t), \theta)}{d\mathbf{x}} - \frac{df_i(\mathbf{x}(t), y(t), \theta)}{d\mathbf{x}} \right] + k(\mathbf{x}, y) \frac{d\tilde{f}_i(\mathbf{x}(t), y(t), \theta)}{dy}.\end{aligned}$$

If we further assume that there is an invertible map from  $(\mathbf{x}, y)$  to  $(\mathbf{x}, g)$ , the last expression implies that  $\frac{dg}{dt} = l(\mathbf{x}, g)$ , and the complete dynamical system therefore has the form

$$\begin{aligned}\frac{d\mathbf{x}}{dt} &= \tilde{\mathbf{f}}(\mathbf{x}, g, \theta) \\ \frac{dg}{dt} &= l(\mathbf{x}, g)\end{aligned}$$

We can therefore distinguish that the system mis-specification corresponds to missing components of the state vector  $\mathbf{x}$ , rather than solely from mis-specification of the form of  $\mathbf{f}$ , by determining that  $dg/dt$  depends on  $g(t)$  as well as being related to  $\mathbf{x}(t)$ .

To apply this criterion in practice, we will actually test for dependence of  $g(t)$  on  $g(t - \delta)$  for some time interval  $\delta$ . If  $g$  is a function of  $\mathbf{x}$ , past values of  $g$  provide no additional information about its present value. However, the state variables of a dynamical system are determined by their past values and the system's laws of motion. For ordinary differential equation models, this idea can be formalized – with appropriate regularity conditions – via the Takens embedding theorem (Takens, 1981), around which a literature in *attractor reconstruction* has been developed (see Arbabanel (1996); Kantz and Schreiber (2005) for an overview). This literature is concerned with estimating system properties purely from data without a proposed model, and the underlying theorems need not necessarily apply



to stochastic systems or systems far away from their limiting behavior (although see Stark et al. (1997) for extensions). However, some of the experience from this literature informs our choice of testing procedure. In particular, the methods predominantly use time-lagged state variables rather than derivatives because the results are more stable (e.g., Kantz and Schreiber, 2005).

Our experience follows this. Because the use of a basis expansion induces a relationship between  $\mathbf{g}(t)$  and its derivative, or between  $\mathbf{g}(t)$  and a short lag. In practice we take  $\delta$  to be larger than the support of the B-spline basis used to estimate  $g(t)$  and in fact use twice the block length employed in the block permutation test. With this in mind, we can state our test of missing components explicitly as

$$H_0 : Eg_i(t) \equiv h(\mathbf{x}(t)) \quad \forall t \text{ versus } H_A : Eg_i(t) \equiv h(\mathbf{x}(t), g_i(t - \delta)) \quad \forall t.$$

We will approach this test using the same ideas as in the previous section. We replace the permutation test by a residual bootstrap based on the model estimated for  $H_0$  within an additional Taylor-series bootstrap for the estimation of  $g_i(t)$  and  $\mathbf{x}(t)$ . Formally, we replace Steps 4c and 4d in the previous section with

- 4c' Using time points  $t_1, \dots, t_K$ , let  $\tilde{\mathbf{g}}_i^b = \mathbf{g}^b(t_i)$  and  $\tilde{\mathbf{x}}_i^b = \mathbf{x}^b(t_i)$ . Estimate models  $\mathbf{h}_1^b(\tilde{\mathbf{x}})$  to predict  $\tilde{g}_i^b$  from  $\tilde{\mathbf{x}}^b$  and  $\mathbf{h}_2^b(\tilde{\mathbf{x}}, \tilde{\mathbf{g}}(t - \delta))$  to predict  $\tilde{g}_i^b$  from  $\tilde{\mathbf{x}}^b$  and  $\mathbf{g}^b(t_{i-1})$  via nonparametric regression. Let  $F_{0b}$  be the  $F$ -statistic between these two models:

$$F_{0b} = \frac{\frac{1}{K} \sum_{i=1}^K \left\| \mathbf{h}_2^b(\tilde{\mathbf{x}}_i^b, \tilde{\mathbf{g}}(t_i - \delta)) - \mathbf{h}_1^b(\tilde{\mathbf{x}}_i^b) \right\|^2}{\frac{1}{K} \sum_{i=1}^k \left\| \tilde{\mathbf{g}}_i^b - \mathbf{h}_2^b(\tilde{\mathbf{x}}_i^b, \tilde{\mathbf{g}}(t_i - \delta)) \right\|^2}.$$

- 4d' (Bootstrap Test) Let  $\hat{g}_i^b$  and  $\epsilon_{\mathbf{g}}^b$  be the predicted values and residuals from  $\mathbf{h}_1^b(\tilde{\mathbf{x}})$ . Loop over  $k = 1, \dots, B_2$ :

- (i) Let  $\epsilon_{\mathbf{g}}^{kb}$  be a permutation of  $\epsilon_{\mathbf{g}}^b$  and  $\tilde{g}_i^{kb} = \hat{g}_i^b + \epsilon_{\mathbf{g}}^{kb}$ .
- (ii) Measure  $F_{kb}$  to be the  $F$ -statistic for a nonparametric regression estimated to predict  $\tilde{g}_i^b$  from  $\tilde{\mathbf{x}}^b$  and  $\mathbf{g}^b(t_i - \delta)$  versus a nonparametric regression estimated to predict  $\tilde{g}_i^b$  from  $\tilde{\mathbf{x}}^b$  only as given in Step 4c'.

This test can thus be run alongside the test for mis-specification in Section 3 at the cost of an extra permutation for each test.

We now have a set of four nested hypotheses concerning the mis-specification of the system which we can write as

$$H1 \quad \mathbf{g}(t) \equiv 0$$

$$H2 \quad Eg(t)|\mathbf{x}(t), \mathbf{g}(t - \delta) \equiv 0$$

$$H3 \quad Eg(t)|\mathbf{x}(t), \mathbf{g}(t - \delta) = h(\mathbf{x}(t))$$

$$H4 \quad Eg(t)|\mathbf{x}(t), \mathbf{g}(t - \delta) = l(\mathbf{x}(t), \mathbf{g}(t - \delta))$$

where in this paper we have provided tests to distinguish H3 from H2 and H4 from H3. Hooker (2009) presents methods to distinguish H2 from H1. We now examine the performance of these tests using simulations and real data.

## 5 Simulation Example: Linear Systems versus van der Pol and Rössler Systems

Our first experiment uses a 2-dimensional linear system:

$$\begin{aligned}\frac{dx_1}{dt} &= a_{11}x_1 + a_{12}x_2 \\ \frac{dx_2}{dt} &= a_{21}x_1 + a_{22}x_2\end{aligned}$$

as a proposed model with the  $a_{ij}$  treated as unknown parameters. We examine three data generating models:

1. Circular motion which corresponds to the linear model with  $(a_{11}, a_{12}, a_{21}, a_{22}) = (0, -1, 1, 0)$  and thus leaves the model correctly specified.
2. The van der Pol oscillator (van der Pol, 1927):

$$\begin{aligned}\frac{dx_1}{dt} &= ax_2 \\ \frac{dx_2}{dt} &= b \left( x_2 - x_1 - \frac{x_2^3}{3} \right)\end{aligned}$$

in which mis-specification appears as an additive term in the equation for  $x_2$  and we take  $(a, b) = (0.25, 4)$ .

3. The Rössler system (Rössler, 1976):

$$\begin{aligned}\frac{dx_1}{dt} &= -x_2 - z \\ \frac{dx_2}{dt} &= x_1 + ax_2 \\ \frac{dz}{dt} &= b + z(x - c)\end{aligned}$$

in which  $z$  represents a separate state variable to be discovered and we take  $(a, b, c) = (0.2, 0.2, 3)$ . These are parameter values classically chosen to produce chaotic dynamics.

For each of these we will examine data generated from the differential equation and from a stochastic differential equation with additive noise corresponding to

$$d\mathbf{x} = \mathbf{f}(\mathbf{x}, \theta)dt + \sigma d\mathbf{W} \tag{7}$$

where  $\mathbf{W}$  is a multivariate Wiener process with independent components. We took  $\sigma^2 = 0.01$  for the linear and van der Pol models and  $\sigma^2 = 0.004$  for the Rössler system. These choices gave us a range of stochastic variabilities without making the non-linear systems diverge to infinity. For each of these, we also added Gaussian observational noise to the value of the system at 220 equally spaced time points from  $t = 0$  to 55. These were given variances of 0.25, 0.001 and 0.01 for the linear, van der Pol and Rössler systems respectively to provide a range of noise levels.  $g(t)$  was added to the second dimension of the system of each model.

Plots of visual diagnostics for system lack of fit from data sets generated in this manner are given in Figure 2. We also report the power of the test in each system in Table 1. Here we observe that our tests are generally conservative. This is likely a result of the bootstrap procedure and the Taylor series approximations. However, our tests do have reasonable power to detect relevant types of mis-specification in these models.

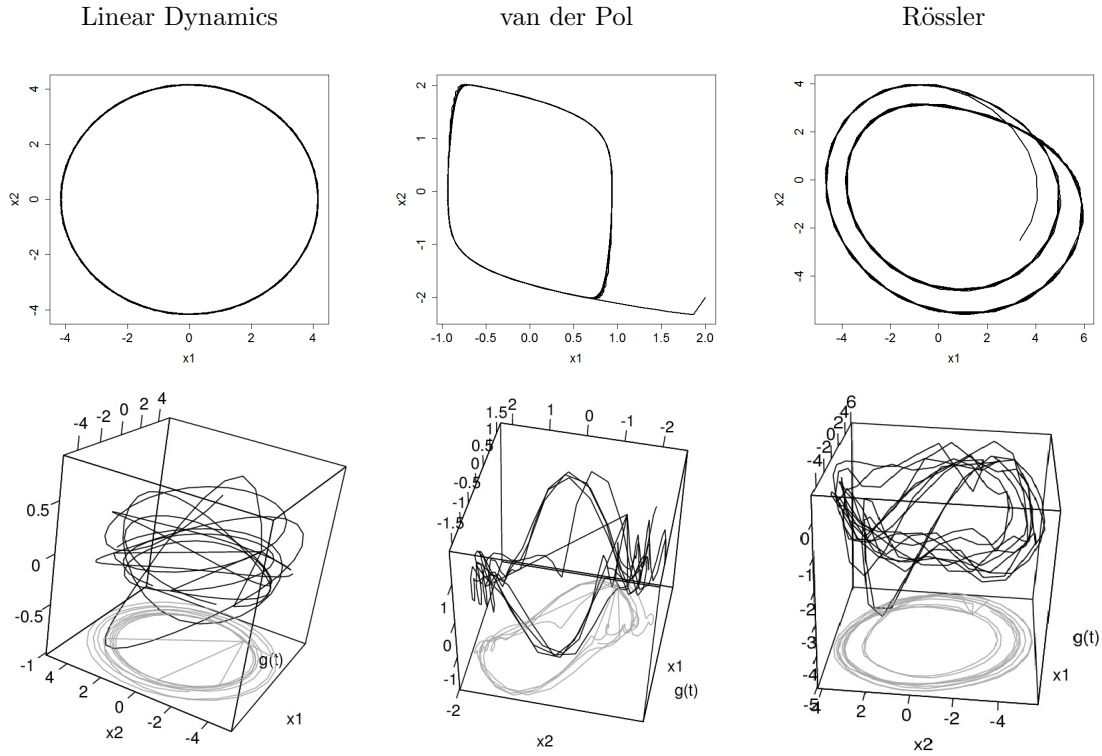


Figure 2: Diagnosing lack of fit for the linear, van der Pol and Rössler ODE systems. Top row: phase plane plots of the two state variables  $x_1, x_2$  that were sampled to create the data series. Bottom, diagnostic plots from the corresponding stochastic models (7). Black curves are the three-dimensional trajectories of the stochastic models, and the grey curves are their projections onto the  $(x_1, x_2)$  plane.

		Linear Dynamics	van der Pol	Rössler
ODE model	Case 2 test	0	1	1
	Case 3 test	0	0	0.59
SDE model	Case 2 test	0	0.895	0.92
	Case 3 test	0.2	0.005	0.27

Table 1: Power of goodness of fit test for Case 2 and Case 3 mis-specification in linear, van der Pol and Rössler ODE and SDE models

## 6 Example: Chemostat Models

In this section, we present the application of these tests to assess evidence for evolution in the chemostat models described in the introduction and given in Figure 1 employing the Rosensweig-MacArthur model (4). Figure 3 presents the estimated time-varying trait plotted against the estimated  $C(t)$  and  $B(t)$  along with a surface representing the smooth of this relationship and predictions from a model that also includes  $p(t-\delta)$ . There is apparent mis-specification of  $\mathbf{f}$ , although the  $p$ -value for this (0.052) falls short of the traditional threshold for significance. There is insufficient evidence ( $p = 0.45$ ) that the state variable is missing a component that could be produced by an additional algal population.

However, these results do not warrant the conclusion that evolution does not occur in this system. The power of these tests rely on the system producing behaviors in which this type of dependence can be readily uncovered, and for this type of system, the power to detect lack of fit is very low. To demonstrate this, we conducted a simulation study based on two plausible, more complex, stochastic models for the rotifer-algae system. Details of these models are given in Appendix A. The salient distinction between the two models is that one of them includes two populations of algae while the other does not. We again simulated 200 data sets from each and conducted the proposed tests on each. Figure 4 presents histograms of the  $p$ -values for each test along with example plots relating  $p(t)$  to  $B(t)$  and  $C(t)$  in each model. Here we see that mis-specification of  $\mathbf{f}$  is detectable ( $\alpha = 0.53$ ) in the two algal population model, but the test for missing state variables has very little power ( $\alpha = 0$  in both models). The diagnostic plots of Figure 4 are helpful in explaining why this is the case; the grey lines produce the design of covariates values for the Case 2 regression of  $p(t)$  on  $(C(t), B(t))$ . Here we see that while the model that incorporates multiple algal types produces cycles which are much more elongated, the cycles still do not cross (as they do in the Rössler system in Figure 2). This means that an appropriate nonlinear dependence of  $p(t)$  on  $(C(t), B(t))$  will capture all of the signal in this relationship, so adding  $p(t - \delta)$  as a covariate will not improve predictive performance.

This example provides the important practical lesson that detection of missing state variables requires the system to behave in ways that cannot be replicated by *any dynamical model* that uses the current state space. We hypothesize that this is possible in the present case because the predator's feeding rate equation can be modified so that predator abundance serves as a proxy for predator age structure, allowing the model to behave like models with predator age structure that can exhibit the kind of antiphase cycles seen in the experiment as a result of predator age structure. Independent experimental evidence tells us the predator age structure is not the mechanism operating in the experiments, but from the time series alone it may not be possible to determine that the actual mechanism involves additional state variables.

We also undertook 200 simulations employing the ODE model (4), transformed to represent  $\log C(t)$  and  $\log B(t)$ , to generate data along with additive Gaussian errors with variance 0.25. This provides a means of checking that the nonlinearity of these equations does not distort our tests. The level of both tests were estimated from this simulation at 0, indicating that the test remains conservative in the presence of nonlinearities.

## 7 Example: Cardiogram Data and the van der Pol System

In this section, we present data from electro-cardiogram measurements obtained from the MIT-BIH Arrhythmia Database (subject 214, Goldberger et al., 2000; Moody and Mark, 2001), given in the first plot of Figure 5. These data will illustrate how our methods can be applied with alternative parameter estimation methodologies. Because of the amount of data (2000 data points are shown in Figure 5), profiling becomes computationally intensive. Instead, we will employ a technique known as gradient matching Ellner et al. (2002), or two-stage least squares Wu et al. (2012) in which we first smooth these data and then choose parameters so that the right hand side of a proposed ODE matches the smooth as well as possible.

Specifically, we employ an alternative formulation of the van der Pol model studied in Section 5

Mis-specification of  $\mathbf{f}$  p-value: 0.052 Mis-specification of  $\mathbf{x}$  p-value: 0.43

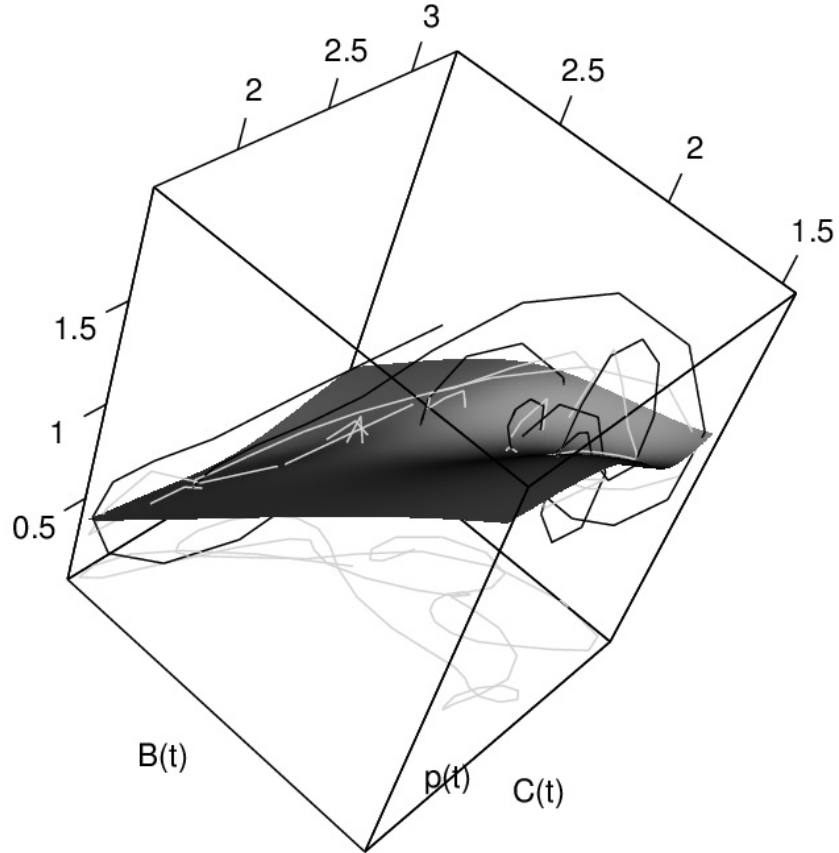


Figure 3: Visualization of the diagnostic tests for the Rosenzweig-MacArthur model applied to the chemostat data. Surface indicates predictions of a model for  $p(t)$  based only on  $(C(t), B(t))$ , dark lines  $p(t)$  plotted against  $(C(t), B(t))$ , light lines: predictions based also on  $p(t - \delta)$ .

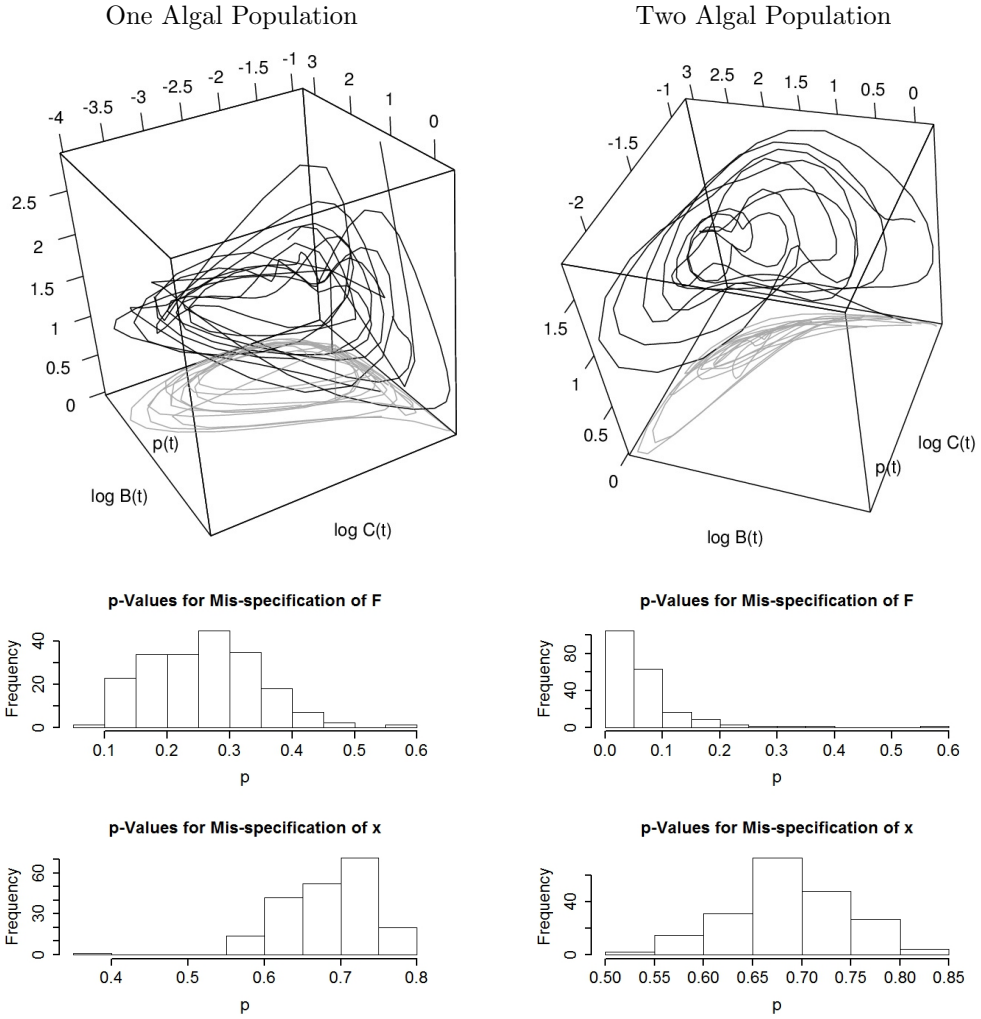


Figure 4: Top row: example diagnostic plots for a Rosenzweig-MacArthur model with only one algal population fitted to data from a chemostat system model with either one algal population (left) or two algal populations (right). Bottom: histograms of  $p$ -values tests for mis-specification of the dynamics  $f$  (top), and mis-specification of the state vector (bottom), based on 200 simulations.

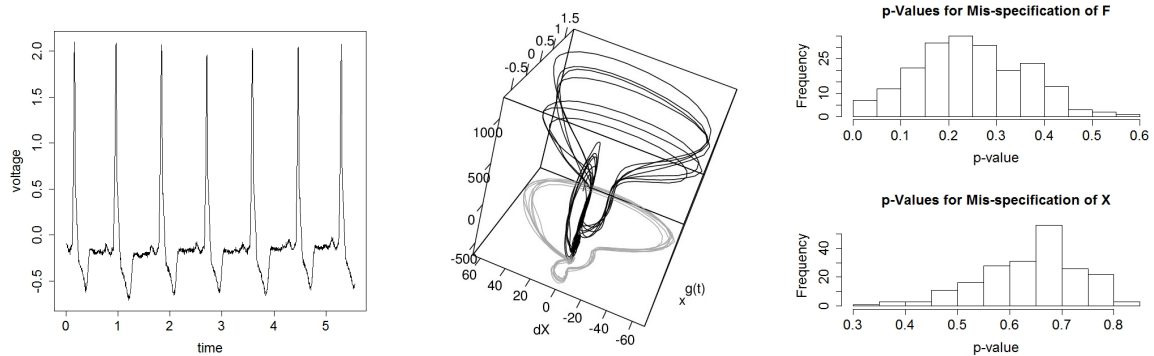


Figure 5: Left: electrocardiogram data. Middle: diagnostic plots for the van der Pol model indicating both Case 2 and Case 3 mis-specification. Right: histograms of  $p$ -values for data simulated from a van der Pol model without mis-specification.

that is given as a second-order differential equation

$$\frac{d^2x}{dt^2} = a + b\frac{dx}{dt} + cx + dx^2 + ex\left(\frac{dx}{dt}\right)^2. \quad (8)$$

The original van der Pol model places further restrictions on the parameters  $a$ ,  $b$ ,  $c$ ,  $d$  and  $e$ , but we leave these to be estimated independently. From this, we first smooth the data using a linear smoother to obtain  $\hat{x}$ ,  $d\hat{x}/dt$  and  $d^2\hat{x}/dt^2$ . We then choose parameters to minimize

$$\int \left( \frac{d^2\hat{x}}{dt^2} - a - b\frac{d\hat{x}}{dt} - c\hat{x} - d\hat{x}^2 - e\hat{x}\left(\frac{d\hat{x}}{dt}\right)^2 \right)^2 dt$$

This can be carried out by evaluating the estimated smooth and its derivatives at a fine grid of time points and then employing linear regression. Following this, the residuals are smoothed using an unpenalized basis expansion to obtain an estimated  $g(t)$  as a lack of fit forcing function.

These steps are all linear operations and can be carried out much more efficiently than generalized profiling allows. After this, the testing procedure proceeds as above with model mis-specification obtained by relating  $g(t)$  to  $x(t)$  and  $dx/dt$  and tests for missing state variables carried out by testing whether  $g(t - \delta)$  provides additional predictive accuracy.

In these data we left off the first and last 100 time points in the testing procedure to remove edge effects and used blocks of size 50. We bootstrapped residuals from the smooth to construct each new data set. Here both tests returned  $p$ -values of zero, indicating that both types of mis-specification were present. In the second plot in Figure 5, the missing dynamic component is only relevant in the “knot” observable where  $g(t)$  undergoes a sub-cycle when plotted against  $x(t)$  and  $dx/dt$ .

To ensure that this effect was not an artifact of the estimation methodology, we conducted a simulation study employing solutions to (8) with additive observation noise. Histograms of  $p$ -values from both tests are given in the final plot of Figure 5 where we observe that although these are not uniformly distributed, the level of the test is at least conservative (0.035 for Case 2, 0 for Case 3).

## 8 Conclusions

This paper represents lack of fit in differential equation models as a series of nested models:

1. No lack of fit

2. Unaccounted-for stochastic variation
3. Mis-specified right-hand side functions for the differential equation
4. Missing or mis-specified state variables that describe the system

and presents test to distinguish the third from the second and the fourth from the third of these. This nested structure is necessary for the last two possibilities but nesting the second and third is not strictly required. However, we believe this nesting makes sense in analogy to regression model diagnostics which include a random error term.

Our tests rely on bootstrap and permutation methodologies in order to require as few assumptions as possible. This leads to their being very conservative at the null hypothesis; it also makes conducting them computationally demanding. However, they are still capable of distinguishing meaningful differences between models, as our simulations indicate. While our methods are based on explicitly smooth models of dynamics, we have also demonstrated that these systems work well with non-smooth diffusion processes.

The non-parametric nature of these tests can reduce their power. As our ecological example indicates, genuinely three-dimensional systems can often be represented as two-dimensional systems, unless they have behavior that cannot be embedded in two dimensions. More powerful tests can be based on specific alternative hypotheses. For example, the two-algal-population model (10) provides better qualitative agreement with the data than does (9). However, neither model is exactly correct, and tests to distinguish between them while making few assumptions about the form of a stochastic model have yet to be developed.

There is also room to design experiments that would yield behavior in which missing state variables, such as the second algal population in the chemostat data, is more readily detected by the tests proposed here. Hooker et al. (2013); Thorbergsson and Hooker (2013) present some initial design of experiments methods for dynamical systems models, but more work is needed to adapt them to this purpose. The power of our test for mis-specified state variables also might be higher when several trajectories have been observed that have different initial values. The test fails when the trajectory of an  $n$  dimensional system, projected onto  $n - k$  dimensions, can be reproduced or approximated well by the solution of some  $n - k$  dimensional dynamical system. This is especially likely if the observed trajectory is on or near a low-dimensional attractor for the dynamics. A second trajectory of the  $n$ -dimensional system, with initial values far from the attractor, might require a different lower-dimensional system to reproduce it, which would reveal that the system is actually higher dimensional.

## References

- Arbabanel, H. D. I. (1996). *Analysis of Observed Chaotic Data*. New York: Springer.
- Arora, N. and L. T. Biegler (2004). A trust region SQP algorithm for equality constrained parameter estimation with simple parametric bounds. *Computational Optimization and Applications* 28, 51–86.
- Bates, D. M. and D. B. Watts (1988). *Nonlinear Regression Analysis and Its Applications*. New York: Wiley.
- Becks, L., S. P. Ellner, L. E. Jones, and N. G. Hairston (2010). Reduction of adaptive genetic diversity radically alters eco-evolutionary community dynamics. *Ecology Letters* 13, 989–997.
- Bellman, R. and R. S. Roth (1971). The use of splines with unknown end points in the identification of systems. *Journal of Mathematical Analysis and Applications* 34, 26–33.
- Bock, H. G. (1983). Recent advances in parameter identification techniques for ODE. In P. Deuffhard and E. Harrier (Eds.), *Numerical Treatment of Inverse Problems in Differential and Integral Equations*, pp. 95–121. Basel: Birkhäuser.



- Ellner, S. P., Y. Seifu, and R. H. Smith (2002). Fitting Population Dynamic Models to Time-Series Data by Gradient Matching. *Ecology* 83(8), 2256–2270.
- Fan, J. and Q. Yao (2008). *Nonlinear Time Series: Nonparametric and Parametric Methods*. Springer Series in Statistics. Springer.
- Girolami, M., B. Calderhead, and S. A. Chin (2011). Riemannian manifold Hamiltonian Monte Carlo. *Journal of the Royal Statistical Society* 73(2).
- Goldberger, A. L., L. A. Amaral, L. Glass, J. M. Hausdorff, P. C. Ivanov, R. G. Mark, J. E. Mietus, M. G. B., C.-K. Peng, and H. E. Stanley (2000). Physiobank, physiotoolkit, and physionet: Components of a new research resource for complex physiologic signals. *Circulation* 101(23), e215–e220.
- Golightly, A. and D. J. Wilkinson (2011). Bayesian parameter inference for stochastic biochemical network models using particle Markov chain Monte Carlo. *Interface focus* 1(6), 1–14.
- Gouriéroux, C. and A. Monfort (1997). *Simulation-based Econometric Methods*. OUP/CORE Lecture Series. OUP Oxford.
- Hooker, G. (2009). Forcing function diagnostics for nonlinear dynamics. *Biometrics* 65, 613–620.
- Hooker, G., K. K. Lin, and B. Rogers (2013). Control theory and experimental design in diffusion processes. *under review*.
- Hooker, G., L. Xiao, and J. Ramsay (2010). *CollocInfer: Collocation Inference for Dynamic Systems*. R package version 0.1.1.
- Ionides, E. L., C. Bretó, and A. A. King (2006). Inference for nonlinear dynamical systems. *Proceedings of the National Academy of Sciences* 103, 18438–18443.
- Kantz, H. and T. Schreiber (2005). *Nonlinear Time Series Analysis*. Cambridge: Cambridge University Press.
- Moody, G. B. and R. G. Mark (2001). The impact of the mit-bih arrhythmia database. *IEEE Engineering in Medicine and Biology* 20(3), 45–50.
- Pascual, M. and S. P. Ellner (2000). Linking ecological patterns to environmental forcing via nonlinear time series models. *Ecology* 81(10), 2767–2780.
- Ramsay, J. O., G. Hooker, D. Campbell, and J. Cao (2007). Parameter estimation in differential equations: A generalized smoothing approach. *Journal of the Royal Statistical Society, Series B* 16, 741–796.
- Ratmann, O., C. Andrieu, C. Wiuf, and S. Richardson (2009). Model criticism based on likelihood-free inference , with an application to protein network evolution. *Proceedings of the National Academies of Sciences* 106(26), 10576–10581.
- Reuman, D. C., R. A. Desharnais, R. F. Costantino, O. S. Ahmad, and J. E. Cohen (2006). Power spectra reveal the influence of stochasticity on nonlinear population dynamics. *Proceedings of the National Academies of Sciences* 103(49), 18660–18665.
- Rössler, O. E. (1976). An equation for continuous chaos. *Physics Letters* 57A(5), 397–398.
- Stark, J., D. S. Broomhead, M. E. Davis, and J. Huke (1997). Takens embedding theorems for forced and stochastic systems. *Nonlinear Analysis, Theory, Methods and Applications* 30(8), 5303–5314.
- Takens, F. (1981). *Detecting Strange Attractors in Turbulence*, pp. 366. Berlin: Springer.

- Thorbergsson, L. and G. Hooker (2013). Experimental design for partially observed markov decision processes. *under review*.
- Tien, J. H. and J. Guckenheimer (2008). *Journal of Computational Neuroscience* 24(3), 358–373.
- van der Pol, B. (1927). On relaxation-oscillations. *The London, Edinburgh and Dublin Philosophical Magazine and Journal of Science* 2(7), 978–992.
- Varah, J. M. (1982). A spline least squares method for numerical parameter estimation in differential equations. *SIAM Journal on Scientific Computing* 3, 28–46.
- Wilson, H. R. (1999). *Spikes, Decisions and Actions: The Dynamical Foundations of Neuroscience*. Oxford: Oxford University Press.
- Wood, S. (2013). *mgcv: Mixed GAM Computation Vehicle with GCV/AIC/REML smoothness estimation*. R package version 1.7-27.
- Wood, S. N. (2010). Statistical inference for noisy nonlinear ecological dynamic systems. *Nature* 466(August).
- Wu, H., H. Xue, and A. Kumar (2012). Numerical discretization-based estimation methods for ordinary differential equation models via penalized spline smoothing with applications in biomedical research. *Biometrics* 68(2), 344–52.
- Yoshida, T., L. E. Jones, S. P. Ellner, G. F. Fussmann, and N. G. Hairston (2003). Rapid evolution drives ecological dynamics in a predator-prey system. *Nature* 424, 303–306.

## A Models for Chemostat Ecological Microcosms

This appendix details the models we used to simulate data in Section 6. These were developed from first principles and independent experimental data (e.g., experiments on predator feeding rates as a function of prey abundance) to describe the experiments which are conducted in chemostat systems; see, for example, Yoshida et al. (2003); Becks et al. (2010).

The experimental system is an approximately cylindrical glass vessel containing growth medium and the cultured organisms, algae and rotifers (bacteria are sometimes also present at very low numbers, but we neglect them here). Growth of algae in the experimental system is limited by Nitrogen concentration ( $N$ ), which is modeled as an additional state variable; all other requirements for algal growth are supplied in excess in the growth medium. In order to support continual algal growth, medium with nitrogen concentration  $N_I$  is added to the chemostat at rate  $\delta$  while its contents are also removed at the same rate. That is, the daily inflow and outflow volumes are both  $\delta$  times the volume of medium in the chemostat.

The additional state variables are algae ( $C$ ) which consume  $N$  in order to reproduce, and two types of rotifer which consume the algae: breeding ( $B$ ) and senescent ( $S$ ). Newborn rotifers are breeding, and they senesce into the  $S$  state at rate  $\lambda$ . Senescent rotifers continue to eat algae, but do not reproduce. The system is well-mixed (by bubbling and/or a magnetic stirrer), so all state variables are removed from the chemostat at rate  $\delta$ .

The one-algal-population model is then described by the equations:

$$\begin{aligned}
\frac{dN}{dt} &= \delta(N_I - N) - \frac{\rho CN}{K_C + N} \\
\frac{dC}{dt} &= C \left[ \frac{\chi_C(t)\rho N}{K_C + N} - \frac{G(B + S)}{K_B + \max(C, Q^*)} - \delta \right], \\
\frac{dB}{dt} &= B \left[ \frac{\chi_B(t)GC}{K_B + \max(C, Q^*)} - (\delta + m + \lambda) \right] \\
\frac{dS}{dt} &= \lambda B - (\delta + m)S.
\end{aligned} \tag{9}$$

The first term in  $dN/dt$  represents the input of Nitrogen at rate  $\delta N_I$  and removal at rate  $\delta N$ , while the second term describes consumption by algae at maximal rate  $\rho$  with saturation constant  $K_C$ . In the equation for  $dC/dt$ , consumed nitrogen is converted into new algae with conversion rate  $\chi_C(t)$  and the algae are predated by both  $B$  and  $S$  with maximal rate  $G$  and half-saturation  $K_B$  subject to a lower limit  $Q^*$  (which puts a “kink” in the predation curve). They are also removed at rate  $\delta$ . In the third equation, breeding rotifers convert consumed algae into  $B$  at rate  $\chi_B(t)$ , while they also senesce at rate  $\lambda$  die at rate  $m$  and are removed at rate  $\delta$ . Finally, senescent rotifers are produced by senescence at rate  $\lambda B$ , die at rate  $m$  and are removed at rate  $\delta$ .

This system is made stochastic by modeling  $\chi_C(t)$  and  $\chi_B(t)$  as geometric Ornstein-Uhlenbeck models:

$$\begin{aligned}
\chi_C(t) &= \chi_C e^{\xi(t)}, \quad d\xi = -a\xi dt + \sigma dW_C \\
\chi_B(t) &= \chi_B e^{\zeta(t)}, \quad d\zeta = -a\zeta dt + \sigma dW_B
\end{aligned}$$

where  $W_B$  and  $W_C$  are independent Weiner processes. This allows the conversion efficiency of algal reproduction to fluctuate around the nominal value, with similar effects for rotifer reproduction.

Observations were simulated as being

$$\mathbf{y}_i = (C + \epsilon_{i1}\sqrt{C}, B + S + \epsilon_{i2}\sqrt{B + S})$$

where  $\epsilon_{i1} \sim N(0, 0.004)$  and  $\epsilon_{i2} \sim N(0, 0.13)$  are independent. This mean-dependent variation mimics Poisson sampling of the chemostat while the differences in variances reflect different population sizes.

Parameters for this model were chosen to be  $\rho = 333$ ,  $\chi_C = 0.0027$ ,  $K_C = 2.2$ ,  $G = 0.009$ ,  $\chi_B = 170$ ,  $K_B = 0.15$ ,  $Q^* = 0.05$ ,  $\sigma = 0.1$  and  $a = 0.5$ . Each run was initialized at initial conditions ( $N_0 = 10$ ,  $C_0 = 0.3$ ,  $B_0 = 10$ ,  $S_0 = 15$ ).

The two algal population model is similar to the one population model. The main difference is that there are two algal state variables  $C_1$  and  $C_2$  which carry out the same functions. The two algal populations have different half-saturation constants  $K_{C_1}$  and  $K_{C_2}$ , and the fraction of the population available for predation is given by  $p_1$  and  $p_2$ ; this occurs in both predation and the saturation effect. Without loss of generality we have taken  $p_1 = 1$  and used the same stochastic conversion parameters as above. Formally, the model is stated as:

$$\begin{aligned}
\frac{dN}{dt} &= \delta(N_I - N) - \frac{\rho C_1 N}{K_{C_1} + N} - \frac{\rho C_2 N}{K_{C_2} + N} \\
\frac{dC_i}{dt} &= C_i \left[ \frac{\chi_C(t)\rho N}{K_{C_i} + N} - \frac{p_i G(B + S)}{K_B + \max(p_1 C_1 + p_2 C_2, Q^*)} - \delta \right], \quad i = 1, 2 \\
\frac{dB}{dt} &= B \left[ \frac{\chi_B(t)G(p_1 C_1 + p_2 C_2)}{K_B + \max(p_1 C_1 + p_2 C_2, Q^*)} - (\delta + m + \lambda) \right] \\
\frac{dS}{dt} &= \lambda B - (\delta + m)S.
\end{aligned} \tag{10}$$

and algal observations were simulated as  $C_1 + C_2 + \epsilon_{i1}\sqrt{C_1 + C_2}$ . Parameters were as above with parameters specific to this model given by  $p_1 = 0.15$ ,  $K_{C_1} = 9$  and  $K_{C_2} = 2.2$ .  $G$  was set to 0.01 to help offset the smaller availability of algae and algal initial conditions were given by  $C_{10} = 0.1$ ,  $C_{20} = 0.2$  for the two algal populations.

